Journal of Nuclear Materials 392 (2009) 396–404

Contents lists available at ScienceDirect

Journal of Nuclear Materials

journal homepage: www.elsevier.com/locate/jnucmat

Determination of the long-term intergranular corrosion rate of stainless steel in concentrated nitric acid

V. Bague, S. Chachoua, Q.T. Tran, P. Fauvet *

CEA, DEN, DPC, SCCME, Laboratoire d'Etude de la Corrosion Non Aqueuse, F-91191 Gif-sur-Yvette, France

ARTICLE INFO

Article history:
Received 17 December 2008
Accepted 19 December 2008

PACS:
81.05.Bx
81.70.−q
82.45.Bb

ABSTRACT

Stainless steels with low carbon content and free from any precipitation undergo intergranular attack in hot nitric acid. The corrosion rate measured by weight loss requires prolonged immersion testing to reach the apparent steady state corrosion, which coincides with the onset of grain dropping. A more appropriate method for predicting the long-term penetration rate is described in this study. A close observation and a statistical analysis of the attack grooves were firstly undertaken using immersion testing. The major findings are an outstanding morphology of the grooves with flat planes and preserved angle even after the onset of grain dropping, as well as a constant rate of the penetration into the surface. The formation of the grooves could then be represented by a geometrical model put forward by Beaunier and co-workers. Consequently, the method proposed for predicting the penetration rate consists in measuring the depth and the angle of the grooves obtained in short time immersion testing. Multiplying the penetration rate calculated from the previous data by the ratio between the penetration depth and the length of the grain boundary path does give an accurate long-term penetration rate. The method has been shown to apply successfully to AISI 304L stainless steel in several nitric solutions.

1. Introduction

Intergranular corrosion is observed on austenitic stainless steels in hot nitric acid even in the absence of chromium carbide precipitates. This type of degradation could be related to the structure and energy of the grain boundaries, as well as to the segregation of some alloying elements in these areas [1–6]. Two states appear to exist during the propagation of the corrosion: the corrosion rate calculated from the weight loss increases with immersion time until a steady state is reached [7–9] which coincides with the onset of grain dropping (Fig. 1). In most cases, at the beginning, the corrosion rate is too slow to reach the steady state with short time experiments performed in laboratory. Therefore, predictions from results obtained with short-term tests could lead to an important underestimation of the long-term corrosion rate.

However, Dunned, Whillock and co. [10–13] emphasized recently that the weight loss is hitherto normalized with respect to the nominal surface area of the test specimen, instead of to the actual area of the metal undergoing corrosion. The latter increases with time and reaches a constant value after the onset of stable grain dropping. Consequently, according to these authors, the apparent increase in the corrosion rate obtained gravimetrically is an artefact. Thus, measurement of the intergranular corrosion rate by weight loss is correct only if the metal is undergoing stable grain dropping. A method for predicting the long-term corrosion rate has been suggested by these authors. It consists in evaluating the weight loss of specimens that undergo pre-corrosion treatment inducing grain dropping. The method allows deconvolution of the corrosion rate with respect to each exposed face by the application of an empirically-determined factor.

The present study details another method to predict the long-term corrosion rate of stainless steel in hot nitric acid from short-term tests. In order to take into account the localized nature of the attack as well as to overcome the difficulties to determine the real area of the metal undergoing intergranular corrosion, the corrosion rate will be straightforwardly calculated from the depths of the attack path.

2. Experimental details

Specimens were machined from a 20 mm thick plate from a single heat of AISI 304L stainless steel with low carbon content and free of chromium carbide precipitates, the composition of which is given in Table 1. Grains are equiaxial. The mean grain size D determined according to the French standard NF A04-102 is about 60 μm. Each specimen is a $30 \times 20 \times 1.5\ mm^3$ parallelepiped. Its surface is wet ground to 2400 grit using SiC paper and is finally polished to a mirror finish using 1 μm diamond powder.

Experiments are immersion tests in nitric media. The test solutions used in this study were sufficiently oxidizing to reach rapidly the steady state corrosion rate, by adding Ce^{4+} oxidizing

* Corresponding author. Tel.: +33 1 69 08 20 24; fax: +33 1 69 08 15 86.
E-mail address: pierre.fauvet@cea.fr (P. Fauvet).

0022-3115/$ - see front matter © 2009 Elsevier B.V. All rights reserved.
doi:10.1016/j.jnucmat.2008.12.100

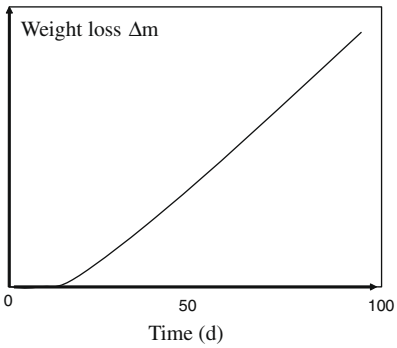

Fig. 1. Weight loss vs. time observed on stainless steel undergoing intergranular corrosion in hot nitric acid.

Table 1
Chemical Composition (wt%) of 304L stainless steel.

Fe	C	Ni	Cr	Mn	Cu	Si	P	S	B	Co
Bal	0.017	10.16	18.34	1.69	0.116	0.57	0.024	0.001	0.0002	0.018

Table 2
Nitric media.

Solution A	8 M HNO_3 + 1 g/L Ce^{4+}
Solution B	8 M HNO_3 + 5 g/L Ce^{4+}

ions (standard potential $E°_{25\,°C}$ = 1610 mV/SHE for the Ce^{4+}/Ce^{3+} couple). The two test solutions are listed in Table 2. Fig. 2 depicts the apparatus used for the immersion tests. Twenty two specimens were suspended in 2000 mL of test solution so that the ratio of the surface area of exposed metal and the liquid volume (i.e. the S/V ratio) is 0.148 cm^{-1}. The solution is continuously renewed with a 42 mL h^{-1} flow rate whereas its temperature is maintained at 100 °C.

One specimen is periodically removed and replaced by a new coupon in order to keep constant the specified S/V ratio. The removed specimen is weighed to determine its weight loss and is examined by optical and scanning electron microscopes. An exhaustive statistical analysis of the parameters of the grooves formed at grain boundaries, i.e., depth, width and angle, is performed from 100 grooves 'nearly symmetrical' (see Section 3) randomly picked up on the specimen cross-section.

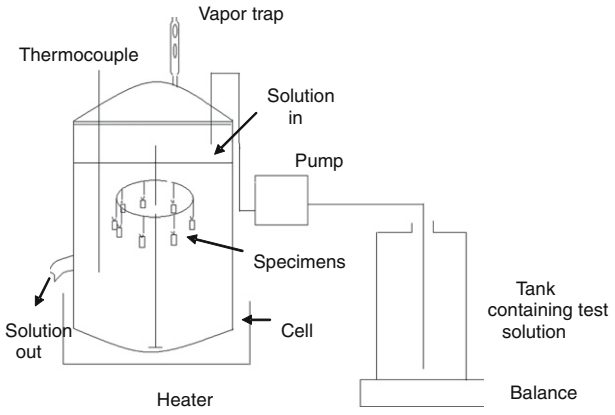

Fig. 2. Schematic immersion test apparatus.

3. Results

Figs. 3–5 show the surfaces of the specimens after various testing times. For every examined specimen, the morphology of the attack has the same features over the whole surface. It suggests that propagation of intergranular corrosion is isotropic. The main features of the degradation are as follows:

1. All grains boundaries are attacked as well as twinning planes (Fig. 3).
2. Opened grooves are formed at boundaries. They have outstanding geometry with two stable planes as sides (Fig. 4). These planes form an angle α which bisector plane is likely the grain boundary surface. Confirmation of these features is apparent on the cross-sections of the grooves which are always triangular and well defined (Fig. 5).
3. Other parameters which characterize the groove dimensions are indicated in Fig. 6. The cases of a dissymmetrical and a symmetrical groove are, respectively, presented on the left and on the right of the figure. The parameters H and L (respectively, H' and L') are the depth and the width of the groove if the initial surface is taken as the reference (respectively, if the final mean surface is taken as the reference).
   H_* (respectively, H'_*) which is the projection of H (respectively, H') on the plane perpendicular to the initial surface, corresponds to the penetration depth. In the case of a symmetrical groove,

$$H = H_*,$$
$$H' = H'_*.$$

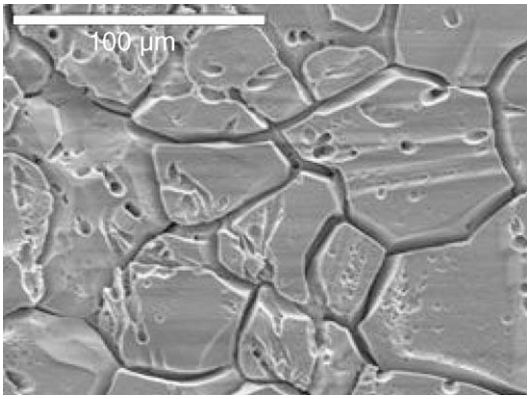

Fig. 3. Surface of 304L SS specimen after 24 h in solution A at 100 °C.

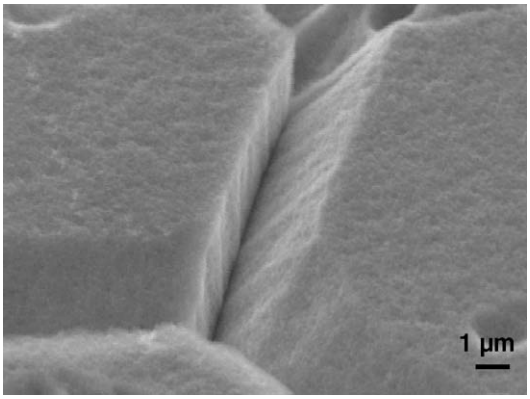

Fig. 4. Observed groove at grain boundary on a 304L SS specimen in solution A at 100 °C.

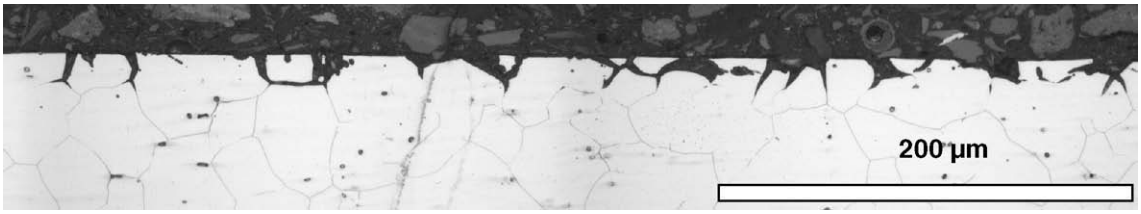

Fig. 5. Cross-section micrograph of a 304L specimen after 7 days in solution B at 100 °C.

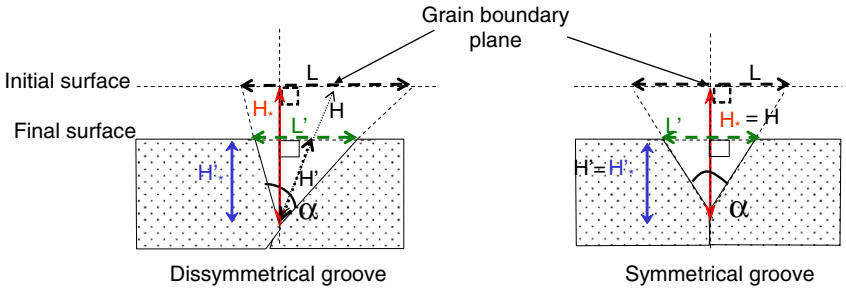

Fig. 6. Schematic groove dimensions.

Symmetrical groove should yield a maximal penetration depth as compared with dissymmetrical groove, as for the same value of H, the former has a higher H_* than the latter. Consequently, only nearly 'symmetrical' grooves with respect to the plane perpendicular to the initial surface (angle difference less than 5°), will be selected for a close statistical analysis of the groove dimensions.

The groove depths H' and the groove angles α follow a Gaussian distribution characterized by their mean value and their standard deviation during the immersion time (Figs. 7 and 8). It suggests that the advancing front of the attack is regular. This feature is actually observed on the specimen's cross-sections (Fig. 5).

4. In addition, during the immersion test, the groove depth H' is never higher than the grain size of the material. It means that the attack doesnot affect deeply the material, in contrast with the morphology of end-grain corrosion [13]. The groove angle is being constant and is roughly 25° for the two test solutions (Figs. 9 and 10).

For a distance shorter than the mean grain size, the groove depth H experiences a linear increase with time immersion (Fig. 11). In addition, a linear change with time of the groove depth H is also observed for the distance longer than the mean grain size. However, the slope of the corresponding plot is smaller. Fig. 12 shows that the weight loss increases also linearly with the immersion time.

4. Discussion

4.1. Formation of groove at grain boundaries according to Beaunier's model

The features of the grooves observed in this study are similar to those observed by Beaunier and co. on 304L stainless steel in 1 M

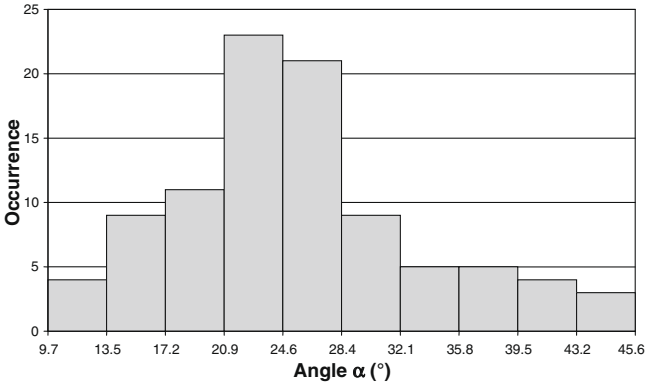

Fig. 8. Distribution of groove angle α after 120 h in solution A.

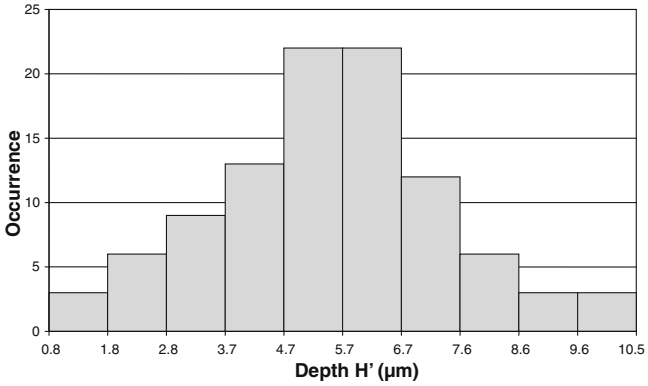

Fig. 7. Distribution of groove depth H' after 120 h in solution A.

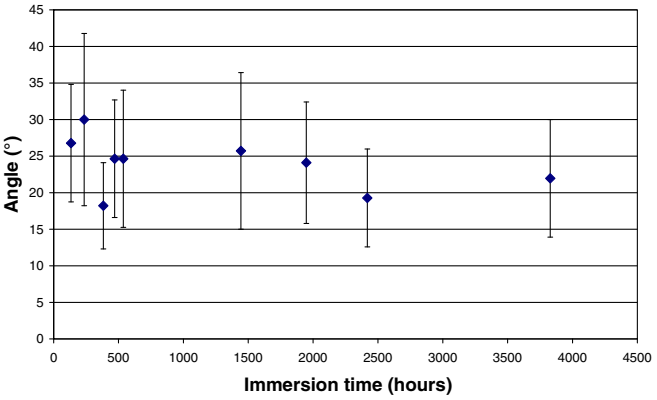

Fig. 9. Groove angle vs. time in solution A.

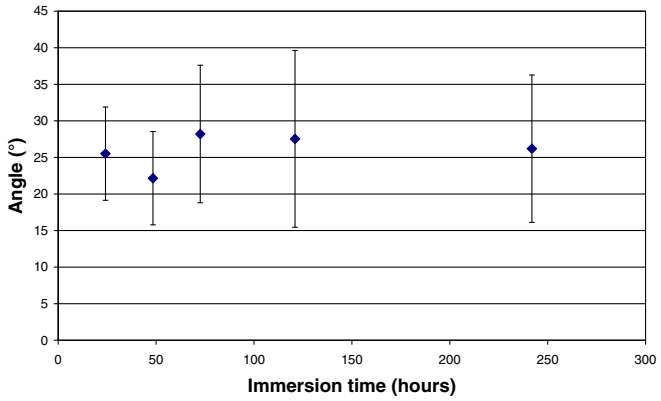

Fig. 10. Groove angle vs. time in solution B.

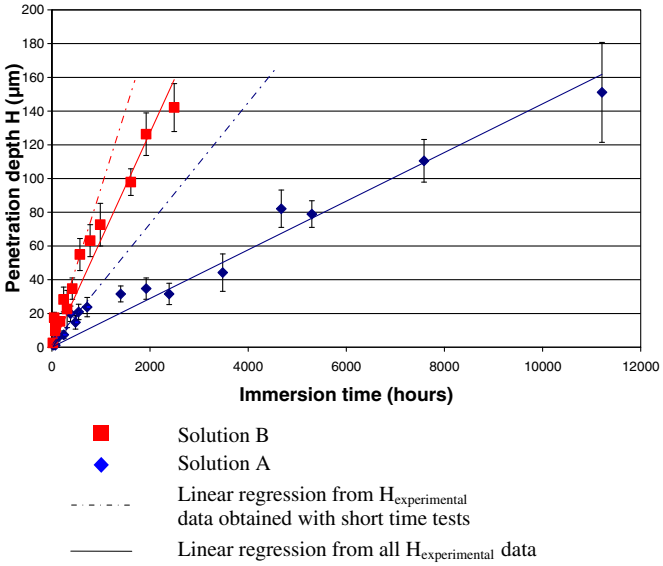

Fig. 11. Observed mean penetration depth H_* vs. time.

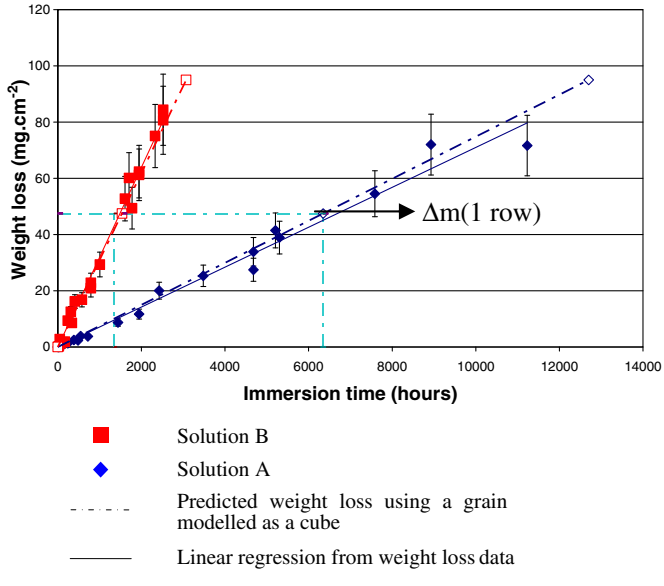

Fig. 12. Weight loss vs. time.

sulphuric acid under potentiostatic polarisation [14–16]. These authors have proposed an electrochemical model for intergranular corrosion under transpassive conditions. It is as if there are *two constant dissolution vectors in equilibrium*: the penetration rate of grain boundary V_g and the dissolution rate of the groove sides and of the specimen surface V_S (Fig. 13). Stable grooves are indeed formed because V_g is higher than V_s. Relation (1) could be then established:

$$\frac{H}{e} = \frac{1}{\sin\frac{\alpha}{2}}, \tag{1}$$

e is the thickness loss due to the uniform corrosion and, as seen later in the chapter, to the grain dropping process.

As H is defined by

$$H = H' + e, \tag{2}$$

Relation (1) gives:

$$H = \frac{H'}{1 - \sin\frac{\alpha}{2}}. \tag{3}$$

Fig. 14 shows the evolution of the groove depth H calculated from relation (3) using experimental data H' and α for the distance shorter than the mean grain size. Since these values match those obtained in this study, the propagation of the intergranular corrosion seems to fit Beaunier's dissolution model.

This type of attack along the grain boundaries must lead to the grain dropping during the propagation of the corrosion. The weight

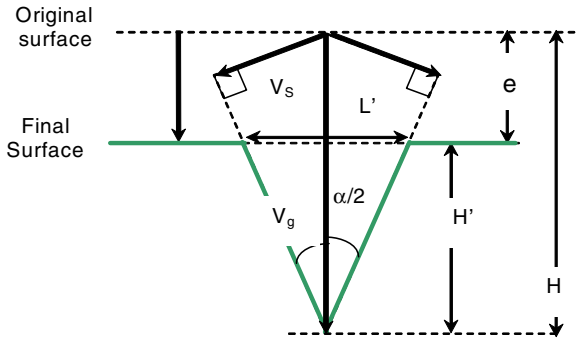

Fig. 13. Schematic groove formation according to Beaunier's model.

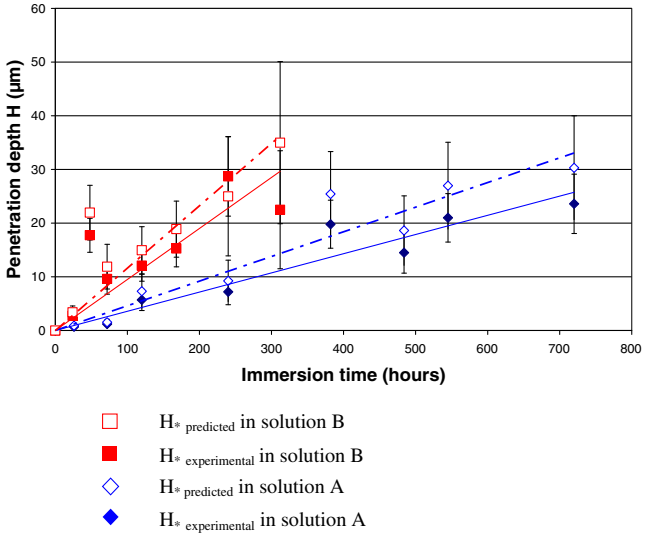

Fig. 14. Observed penetration depth and predicted penetration depth as a function of time.

loss could then be predicted in the following way: equiaxial grain could be represented as a regular cube or a truncated octahedron. Other identical units are then packed to fill the space as shown in Fig. 15. When the advancing front of the intergranular corrosion reaches values between 1.5 D (in the case of a grain shape modelled as a cube) and 1.8 D (in the case of a grain shape modelled as a truncated tetrahedron), one row of grains is broken away from the surface of the specimen. This period of time t varies from 5860 to 6840 h for the solution A (8 M HNO_3 + 1 g/L Ce^{4+}) and from 1390 to 1680 h for the solution B (8 M HNO_3 + 5 g/L Ce^{4+}). The corresponding weight loss is about 47.5 mg/cm^2. The specimen loses one entire row of grains every such interval of time. As the estimated weight loss is actually consistent with a good accuracy with the experimental weight loss data (Fig. 12), grains should drop row by row during the propagation of the intergranular corrosion. Grains are actually observed at the bottom of the corrosion cell (Fig. 16).

The penetration rate $\left(\frac{dH}{dt}\right)_A^{\text{short time}}$ is given by the groove depth-time plot obtained from short time immersion testing, which requires statistical analyses of groove depths. It could also be predicted with only one immersion test. Since the intergranular corrosion rate agrees with Beaunier's dissolution model, we obtain with our experimental results:

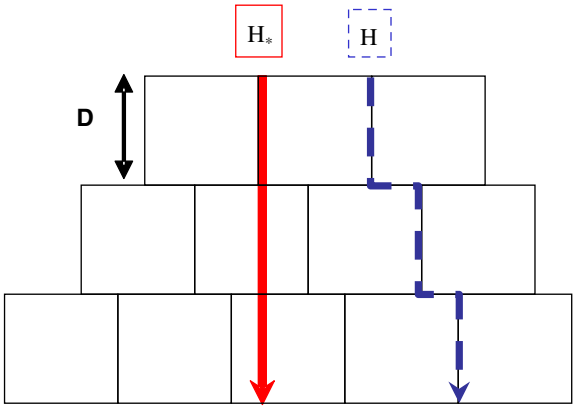

Fig. 15. Difference between the penetration depth H_* and the grain boundary path's length H.

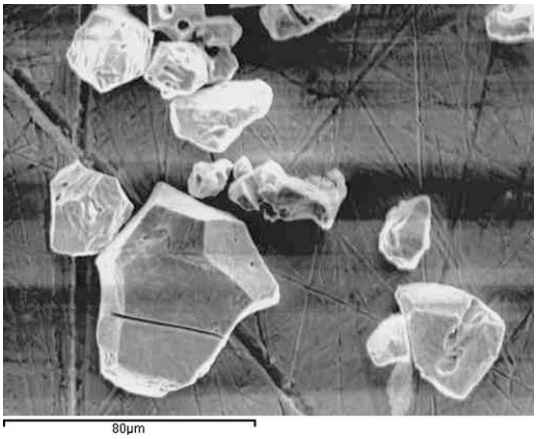

Fig. 16. Grain dropped from 304L SS specimen.

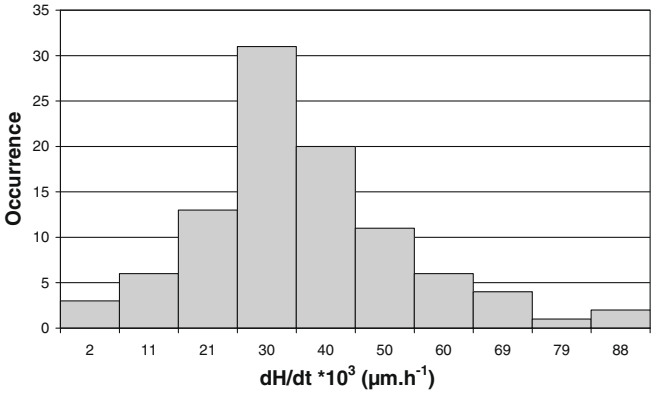

Fig. 17. Distribution of $\left(\frac{dH}{dt}\right)_{\text{experimental}}^{\text{short time}}$ in solution A.

$$\frac{H}{e} = \frac{1}{\sin\frac{\alpha}{2}}, \tag{4}$$

$$\frac{dH}{dt} = \frac{1}{\sin\frac{\alpha}{2}}\frac{de}{dt}. \tag{5}$$

For an angle α between 0 and 60°, $\sin\frac{\alpha}{2}$ is not very different from $\tan\frac{\alpha}{2}$. It can then be replaced by $\tan\frac{\alpha}{2}$ in Relation (5) with an error inferior to 15%:

$$\frac{dH}{dt} = \frac{1}{\sin\frac{\alpha}{2}}\frac{de}{dt} \cong \frac{1}{\tan\frac{\alpha}{2}}\frac{de}{dt} = \frac{1}{\frac{L'/2}{H'}}\frac{de}{dt}, \tag{6}$$

Or

$$\frac{dH}{dt} = \frac{H'}{\frac{L'}{2}}\frac{de}{dt}. \tag{7}$$

In addition,

$$t\frac{de}{dt} + H'(t) = t\frac{dH}{dt}. \tag{8}$$

The combination of (7) and (8) gives:

$$\frac{dH}{dt} = \frac{2[H'(t)]^2}{[2H'(t) - L'(t)]t}. \tag{9}$$

Therefore, the penetration rate $\left(\frac{dH}{dt}\right)_A^{\text{short time}}$ could be determined by relation (10) from one immersion test after a lapse of time t_1:

$$\left(\frac{dH}{dt}\right)_A^{\text{short time}} = \frac{2[H'(t_1)]^2}{[2H'(t_1) - L'(t_1)]t_1}. \tag{10}$$

Such Gaussian distributions of $H'(t)$ and L' give a Gaussian distribution of $\left(\frac{dH}{dt}\right)_{\text{experimetal}}^{\text{short time}}$ (Fig. 17). As seen in Table 3, the $\left(\frac{dH}{dt}\right)_{\text{predicted}}^{\text{short time}}$ obtained is consistent with the slope resulting from the groove depth-time plot.

In conclusion, these results show that the formation of the grooves at grain boundaries agrees with the Beaunier's dissolution model; the propagation of the grooves leads to the periodical 'row by row' grain dropping. Such a type of propagation yields a linear increase in penetration depth H, which is usually observed by other authors [10,12,18].

Table 3
Comparison of $\left(\frac{dH}{dt}\right)_{\text{predicted}}^{\text{short time}}$ (µm/h) determined from groove depth-time plot and from Beaunier's model.

	$\left(\frac{dH}{dt}\right)_{\text{predicted}}^{\text{short time}}$ from groove depth-time plot	$\left(\frac{dH}{dt}\right)_{\text{predicted}}^{\text{short time}}$ from one groove depth according to Beaunier's model
Solution B	0.12 ± 0.008	0.21 ± 0.06
Solution A	0.036 ± 0.002	0.055 ± 0.015

4.2. Determination of the relationship between the penetration depth H'_* and the grain boundary path's length H' affected by intergranular corrosion

Since a linear increase in thickness loss indicates a constant corrosion rate, prediction of the intergranular corrosion rate from groove depth data appears quite easy. However, as seen in Fig. 11, the corrosion rate determined from the short time immersion testing $\frac{dH^{\text{short time}}}{dt}_{\text{experimetal}}$ differs from the corrosion rate determined from long time immersion testing $\frac{dH^{\text{long time}}}{dt}_{\text{experimetal}}$. It is illustrated by the fact that the slopes of the corresponding groove depth-time plots are not similar (Fig. 11). The $\frac{dH^{\text{short time}}}{dt}_{\text{experimetal}}$ is about twice higher than the $\frac{dH^{\text{long time}}}{dt}_{\text{experimetal}}$. This result could be straightforwardly associated with the difference between the penetration depth H'_* and the length of the grain boundary path H'. This idea can be illustrated in Fig. 15 using a very simple two dimensional representation of the grain shape modelled as a cube.

By analogy to the terminology used in the porous media, a correlation factor k, labelled as 'tortuosity' factor, could be defined as:

$$k = \frac{H'_*}{H'}. \tag{11}$$

It represents the ratio between the penetration depth H'_* (in other words the thickness of the metal affected by the intergranular corrosion) and the length of the grain boundary path H' (in other words the real path followed by the intergranular corrosion). In all cases, this ratio must be less than 1 and is expected to be unique for a homogeneous material. The depth penetration could then be simply estimated from Relation (12):

$$H = k\left(\frac{dH}{dt}\right)^{\text{short time}} t. \tag{12}$$

Several methods mainly based on geometrical considerations are examined in order to determine the factor k.

4.2.1. Determination of the tortuosity factor k – Method 1

This method consists in measuring the mean grain boundary path observed on a cross-section of the specimen prepared for metallographic examination. For a distance H'_* randomly chosen, about ten corresponding grain boundary paths H' were measured (Fig. 18). Using the mean value of H', we obtain:

$$k = \frac{H'_*}{H'} = 0.70 \pm 0.01. \tag{13}$$

Fig. 19 shows the penetration depths calculated by using the $\left(\frac{dH}{dt}\right)^{\text{short time}}$ and the factor k. This method provides a better account of the experimental data than does the method using only $\left(\frac{dH}{dt}\right)^{\text{short time}}$. However, the difference between the calculated slope and the experimental slope of the penetration depth-time plot is still quite important, around 67%.

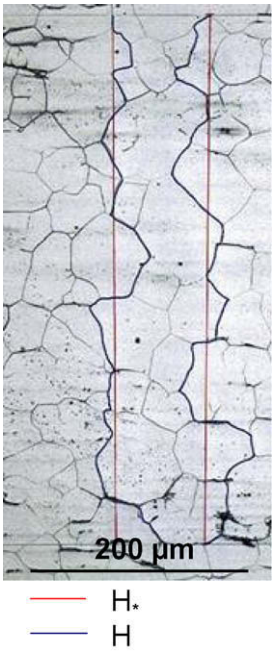

Fig. 18. Cross-section of the specimen.

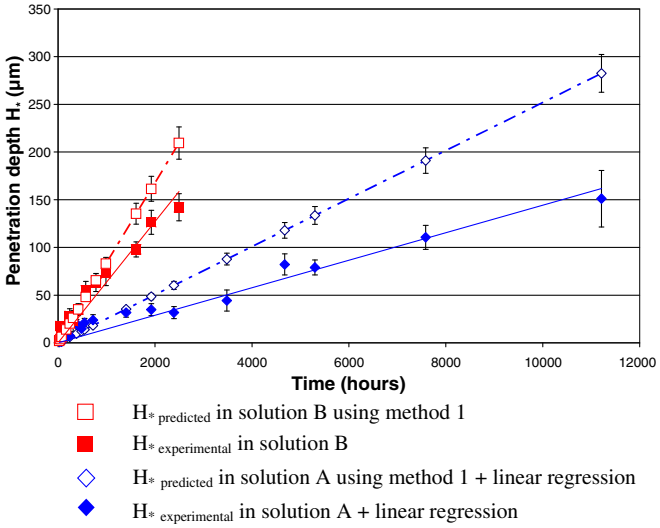

Fig. 19. Penetration depth H_* predicted using method 1.

4.2.2. Determination of the tortuosity factor k – Method 2

The factor k is determined using a representation of grain modelled as truncated octahedron (Fig. 20). For the mean grain size D, the side a of the octahedron is given by:

$$a = \frac{D}{\sqrt{10}}. \tag{14}$$

The longest grain boundary path H', represented by the dotted line in Fig. 20, corresponds to the penetration depth H'_* represented by the unbroken line. These parameters are given by:

$$H'_* = \frac{\sqrt{2} + 2\cos(35°16)}{\sqrt{10}} D, \tag{15}$$

$$H' = \frac{5}{\sqrt{10}} D, \tag{16}$$

$$k = \frac{H'_*}{H'} = \frac{\sqrt{2} + 2\cos(35°16)}{5}. \tag{17}$$

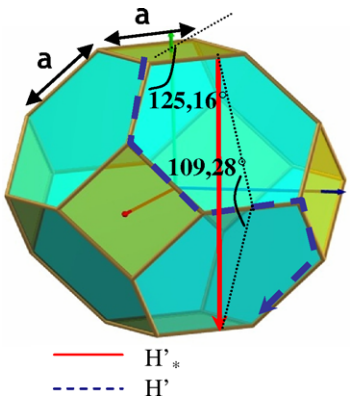

Fig. 20. Grain modelled as truncated octahedron.

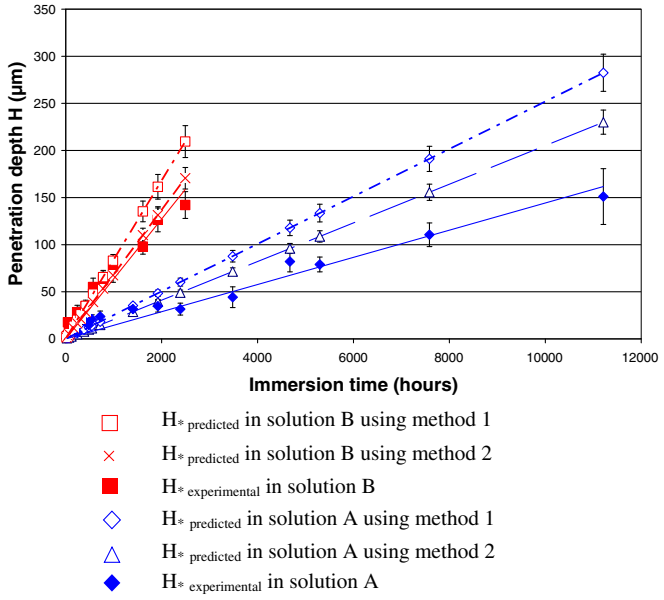

Fig. 21. Penetration depth predicted using method 2 – comparison with method 1.

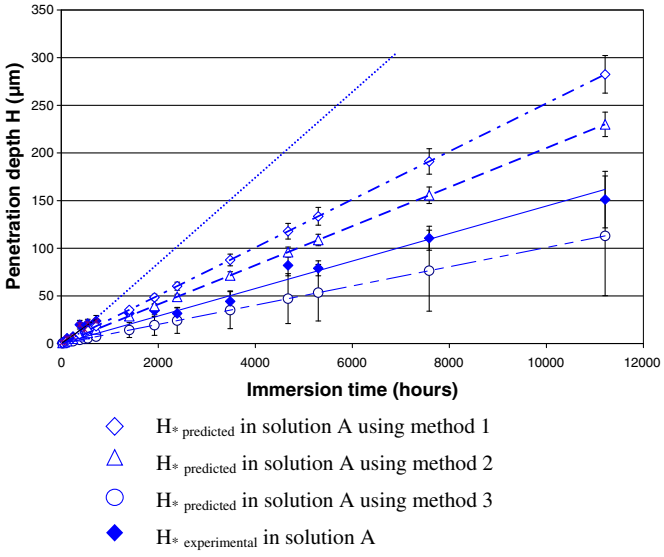

Fig. 22. Penetration depth predicted using method 3 – comparison with methods 1 and 2.

So, the factor k is 0.57. Fig. 21 shows the penetration depth-time plot predicted from the factor k and the value of $\left(\frac{dH}{dt}\right)^{\text{short time}}$. The difference between predicted slope and experimental slope of the plot is not greater than 33%.

4.2.3. Determination of the tortuosity factor k – Method 3

The factor k could also be determined experimentally using a nitric media reference sufficiently oxidizing so that the phase of grain dropping is quickly attained, for example within a month. A solution containing 8 M HNO_3 and 5 g/L of Ce^{4+} (solution B) satisfies such a condition for 304L stainless steel.

A specimen was immersed in this medium and only removed after losing a thickness higher than the mean grain size D. The factor k could then be calculated from the value of $H'_{*\ \text{experimental}}$ measured on the specimen and the value of $H'_{*\ \text{predicted}}$ predicted by the relation (18):

$$H'_{*\ \text{predicted}} = \left(\frac{dH}{dt}\right)_B^{\text{short time}} t. \tag{18}$$

It gives:

$$k = \frac{H'_{\text{experiment}}}{H'_{\text{predicted}}} = 0.34 \pm 0.07. \tag{19}$$

The predicted penetration depth is in agreement with the experimental data (Fig. 22).

4.2.4. Comments

The factor k obtained from these three methods and the $\frac{dH}{dt}^{\text{long time}}_{\text{predicted}}$ corresponding are reviewed and compared to $\frac{dH}{dt}^{\text{long time}}_{\text{experimental}}$ in Table 4 for the solution A. The second and third method give a quite accurate prediction for the $\frac{dH}{dt}^{\text{long time}}$.

As seen in §4.1, the $\left(\frac{dH}{dt}\right)^{\text{short time}}_{\text{predicted}}$ can also be determined using relation (10) according to the Beaunier dissolution's model. By applying the factor k determined using the third method to this value, we obtain $\left(\frac{dH}{dt}\right)^{\text{long time}}_{\text{predicted}}$ for the solution A which is also consistent with $\left(\frac{dH}{dt}\right)^{\text{short time}}_{\text{experimental}}$ data (Table 5 and Fig. 23).

We must emphasize that the factor k determined from the second method doesn't vary with the mean grain size for materials with equiaxial grains. It may indicate that for a material with equiaxial grains, the factor k defined in this study does not depend on the grain size. This information is not opposed to the ideas widely accepted in the literature, which are put forward that grain size has an important influence on the intergranular corrosion rate. In fact, for a given volume of metal, a variation of the grain size induces a variation in grain boundary surface so that the higher is the grain size, the smaller is the intergranular surface. The impurity concentration is constant in the material but impurities are shared out between grain boundary surfaces. Consequently, in most cases, the impurity concentration in the grain boundaries increases with the grain size, so is the intergranular corrosion rate. In our study, the grain size may be without influence on the factor k but the opposite is expected on $\frac{dH}{dt}^{\text{short time}}_{\text{predicted}}$. Further experiments are planned to examine the effect of the grain size upon the factor k and the $\frac{dH}{dt}^{\text{short time}}_{\text{predicted}}$, although we are aware that grain size and impurity concentration might not be independent parameters. Actually, any cold working and heat treatment used for increasing the grain size influences the segregation of impurity in the grain boundaries.

The results obtained in this study are also in agreement with Dunnett's statements on the apparent increase of corrosion rate observed from weight loss data [10]. According to these authors,

Table 4
Comparison of $\left(\frac{dH}{dt}\right)^{\text{long time}}_{\text{predicted}}$ (µm/h) calculated using the factor k for the solution A.

	Method 1	Method 2	Method 3	Experimental
Factor k	0.70 ± 0.01	0.57	0.28 ± 0.14	–
$\frac{dH}{dt}^{\text{short time}}_{\text{experimental}}$	–	–	–	0.036 ± 0.002
$\frac{dH}{dt}^{\text{long time}}_{\text{predicted}}$	0.025 ± 0.002	0.021 ± 0.001	0.010 ± 0.003	–
$\frac{dH}{dt}^{\text{long time}}_{\text{experimental}}$	–	–	–	0.015 ± 0.001

Table 5
$\left(\frac{dH}{dt}\right)^{\text{long time}}_{\text{predicted}}$ (µm/h) determined using k ratio calculated from method 3 and using $\left(\frac{dH}{dt}\right)^{\text{short time}}_{\text{predicted}}$ calculated from Beaunier's model (i.e. the relation (10)).

	Solution B	Solution A
$\left(\frac{dH}{dt}\right)^{\text{short time}}_{\text{predicted}}$	0.215 ± 0.06	0.055 ± 0.015
k	0.30 ± 0.15	0.30 ± 0.15
$\left(\frac{dH}{dt}\right)^{\text{long time}}_{\text{predicted}}$	0.060 ± 0.03	0.014 ± 0.003
$\left(\frac{dH}{dt}\right)^{\text{long time}}_{\text{experimental}}$	0.063 ± 0.03	0.015 ± 0.001

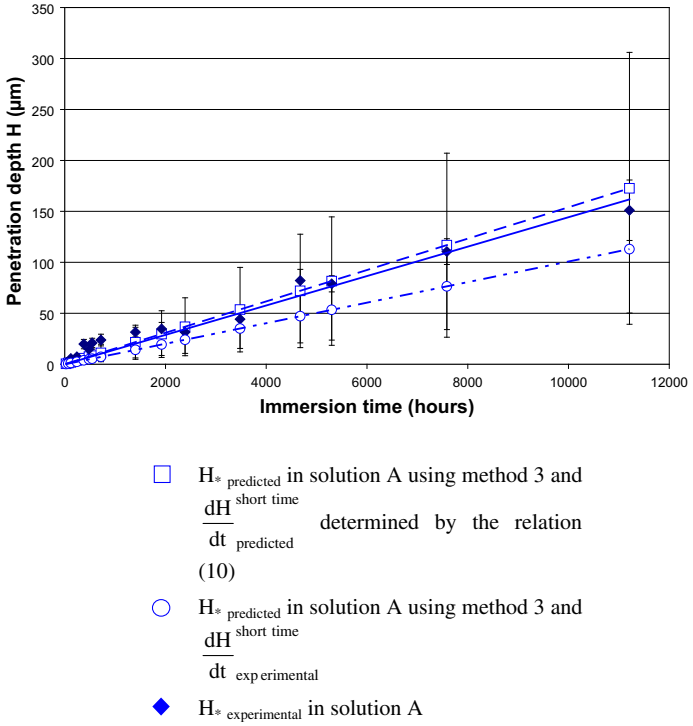

Fig. 23. Penetration depth predicted in solution A (8 M HNO_3 + 1 g/L Ce^{4+}) using the factor k determined from method 3.

the apparent increase in corrosion rate obtained gravimetrically is an artefact since the weight loss is hitherto normalized with respect to the nominal surface area of the test specimen, instead of to the actual area of the metal undergoing corrosion. The latter increases with time up to reach a constant value when grain dropping steady state is achieved (Fig. 24). This idea is not easily conceivable. But, using a two dimensional representation, a simulation of the advancing front according to Beaunier's dissolution model seems to justify a preservation of the surface area of the advancing front after the stable grain dropping, i.e. after the dropping of the first row of grains. As seen in Fig. 25, the surface areas of the interface at $t = \frac{3}{2}\frac{D}{V_g}$, $t = 2\frac{D}{V_g}$ and $t = \frac{5}{2}\frac{D}{V_g}$ are identical. Ohno and co. obtained the same type of interface when they simulate the weight loss promoted by intergranular corrosion [17]. However from our point of view, this result is conclusive only when the material is subject to intergranular corrosion and not to end-grain corrosion [13].

Even if the apparent increase of the weight-loss rate is not seen in the present study, a linear increase of the penetration depth indicates that the intergranular corrosion rate is constant during the propagation of intergranular corrosion.

Finally, the method 2 could be used for materials with equiaxial crystallization while the method 3 may be used for any material.

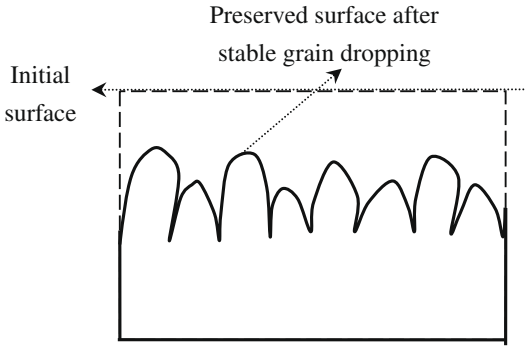

Fig. 24. Schematic surface undergoing intergranular corrosion.

5. Conclusion

This study shows that the propagation of intergranular corrosion of stainless steel such as 304L in hot nitric acid leads to the formation of grooves with outstanding geometry: triangular grooves with regular faces, preserved angle during the propagation of the intergranular corrosion. This morphology is consistent with the grain boundary dissolution model proposed by Beaunier and coll. It is as if there are two constant dissolution vectors in equilibrium, the penetration rate vector of grain boundary V_g and the dissolution rate of the groove faces and of the surface of the specimens V_S.

Statistical analyses as well as an examination of the cross-section of the specimen reveal a regular advancing front. These features of the degradation agree with a grain dropping 'row by row' process. The grain dropping process and the linear increase in groove depth observed on the distance shorter than the mean grain size should result in increasing linearly the penetration depth, which is actually observed in this study.

Consequently, the penetration depth could be simply determined from the short-term penetration rate obtained from short time tests by the application of a factor k, labelled as 'tortuosity' factor; the latter takes into account the 'real' grain boundary path. On one hand, the short-term penetration rate could be calculated either from the groove depth-time plot or from the Beaunier's dissolution model. On the other hand, the factor k could be determined experimentally or by modelling grain shape as truncated octahedron.

Work is in progress to determine whether grain size has a great influence on the factor k and on the penetration rate obtained from short-term tests data.

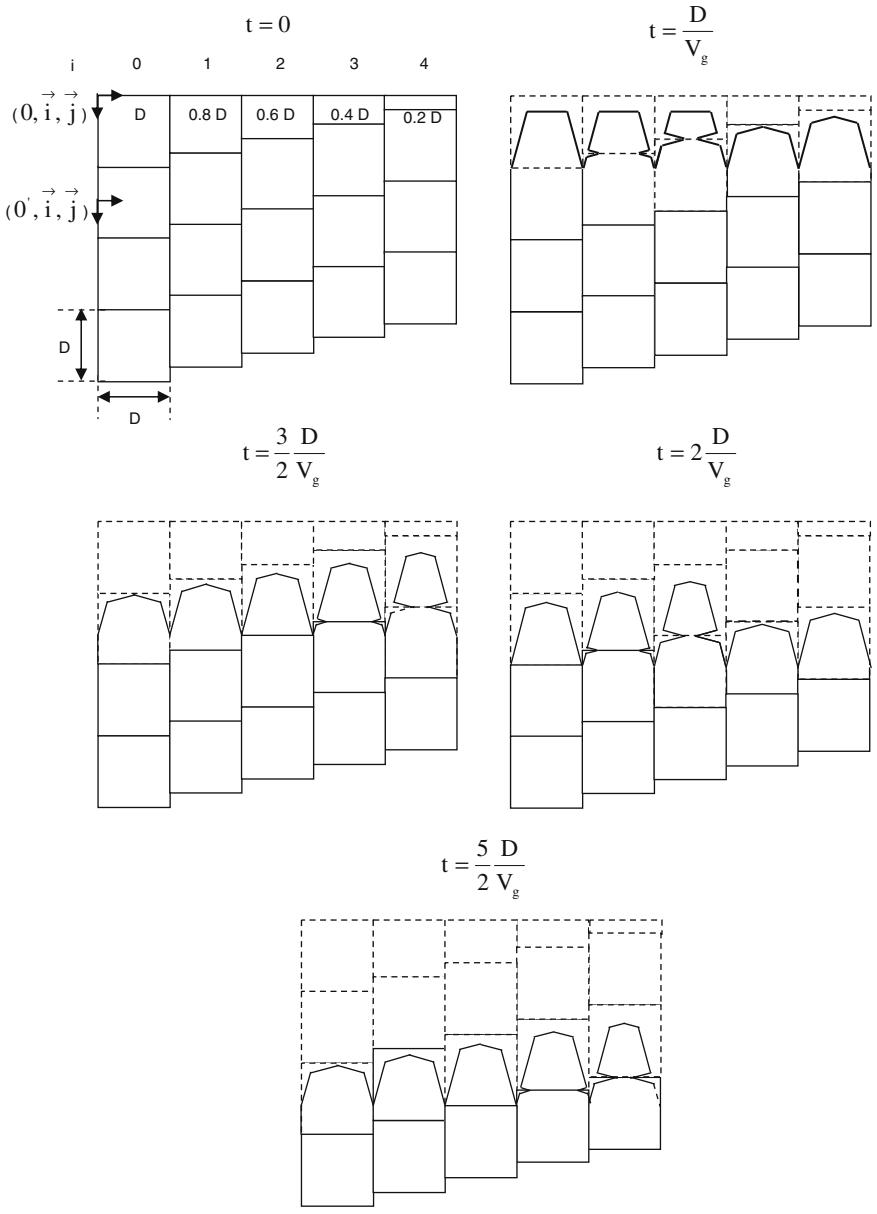

Fig. 25. Simulation of the advancing front for stainless steel undergoing intergranular corrosion in hot nitric acid.

Acknowledgements

This work has been supported by AREVA NC and CEA authorities. We are also grateful to D. Mas, B. Fieulaine, R. Robin, B. Gwinner, F. Balbaud and A. Terlain for their helpful suggestion and assistance during this study.

References

[1] J.S. Armijo, Corrosion 24 (1968) 24.
[2] H. Coriou, A. Desestret, L. Grall, J. Hochman, Mémoires scientifiques Rev. Métallurg LXI (3) (1964) 177.
[3] A. Desestret, I. Epelboin, M. Froment, P. Guiraldenq, Corros. Sci. 18 (1968) 225.
[4] A. Desestret, J. Ferriol, G. Vallier, Mater. Technol. 65 (9–10) (1977) 621.
[5] J. Stolarz, Journal de Physique IV, Colloque C7, supplement to Journal de Physique III 5 (1995) C7-423.
[6] M. Mayuzumi, J. Ohta, K. Kako, Corrosion 56 (2000) 70.
[7] H. Coriou, J. Hure, G. Plante, Electrochim. Acta 5 (1961) 105.
[8] M. Mayuzumi, T. Fujita, Effect of oxidizing ions and heat transfer on the corrosion rates of stainless steels and zirconium in nitric acid, in: Proceedings of International Symposium on Plant Aging and Life Predictions of Corrodible Structures, Sapporo, Japan, 1995, p. 853.
[9] M. Mayuzumi, J. Ohta, T. Arai, Corrosion 54 (1998) 271.
[10] B.F. Dunnett, G.O.H. Whillock, Corrosion 59 (2003) 274.
[11] M. Takeuchi, G.O.H. Whillock, J. Nucl. Sci. Technol. 41 (2004) 702.
[12] G.O.H. Whillock, B.F. Dunnett, Intergranular corrosion testing of austenitic stainless steels in nitric acid solution, in: Proceedings of Eurocorr 2004, Nice, France, 2004.
[13] G.O.H. Whillock, B.F. Dunnett, M. Takeuchi, Corrosion 61 (2005) 58.
[14] L. Beaunier, M. Froment, D. Lepoutre, C. Vignaud, Métaux Corros. Industrie 610 (1976) 211.
[15] L. Beaunier, M. Froment, C. Vignaud, Electrochim. Acta 25 (1980) 1239.
[16] L. Beaunier, Journal de Physique, Colloque C6, supplement to Journal de Physique 43 (12) (1982) C6-271. Tome.
[17] A. Ohno, H. Isoo, M. Akashi, Numerical model for intergranular corrosion rate of stainless steel in nitric acid, in: Proceedings of International Symposium on Plant Aging and Life Predictions of Corrodible Structures, Sapporo, Japan, 1995, p. 869.
[18] H. Coriou, L. Grant, G. Kurka, G. Plante, Influence des ions chrome sur la corosion intergranulaire d'aciers inoxydables austénitiques en milieu nitrique, in: Proceedings of Colloque de Métallurgie, Saclay, France, Vol. IV, 1960, p. 75.